

Gas Detecting Evaluation by Graphitic-based Silicon Carbide Nanosurface doped with Manganese: A Promising Device for Air Pollution Monitoring

Fatemeh Mollaamin^{a,b}

[a] Department of Food Engineering, Faculty of Engineering and Architecture, Kastamonu University, Kastamonu, Turkey

[b] Department of Biology, Faculty of Science, Kastamonu University, Kastamonu, Turkey
E-mail: smollaamin@gmail.com

DOI: 10.29303/aca.v7i1.196

Article info:

Received 18/08/2023

Revised 12/02/2024

Accepted 24/03/2024

Available online
13/04/2024

Abstract: Silicon carbide (SiC) as a direct broad bandgap semiconducting material has the potential to bring a considerable development into optoelectronic and electronic devices. This article aims to investigate Physico-chemical properties of manganese (Mn)-doped graphene-like silicon carbide (SiC) monolayer sheet by the first-principles methods based on the density functional theory (DFT) for scavenging of CO, CO₂, NO, NO₂ gas molecules. The results recommend that the adsorption of these gas molecules on Mn-embedded SiC sheet monolayer is more energetically desired than that on the pristine ones. Gas molecules of CO, CO₂, NO, NO₂ have been adsorbed on the Mn site of doped SiC monolayer through the formation of covalent bonds. The assumption of chemical adsorptions has been approved by the projected density of states (PDOS) and charge density difference plots. Charge density difference calculations also indicate that the electronic densities were mainly accumulated on the adsorbate of CO, CO₂, NO, NO₂ gas molecules. The ability of SiC nanosheet for monitoring of CO, CO₂, NO and NO₂ is fluctuated by their selectivity and sensitivity through NMR, NQR, IR and HOMO/LUMO approaches which can represent the efficiency of Mn-doped SiC surface as the promising sensors toward air pollution detecting.

Keywords: Mn-SiC_sh; CO; CO₂; NO; NO₂; gas detector

Citation: Mollaamin, F. (2024). Gas Detecting Evaluation by Graphitic-based Silicon Carbide Nanosurface doped with Manganese: A Promising Device for Air Pollution Monitoring. *Acta Chimica Asiana*, 7(1), 377–388. <https://doi.org/10.29303/aca.v7i1.171>

INTRODUCTION

Graphene with two-dimensional (2D) layered physical structure and the unique electronic properties has simulated a broad range of research enthusiasm on 2D materials which can be applied for the electronic, optoelectronic, and spintronic devices [1–5].

But, the practical application of 2D material like graphene might be confined with small band gap. Thus, new 2D materials with perfect mechanical, thermoelectric, optical and electronic properties are the clue to the recent scientific investigations [6–9].

In transition metal (TM) decorated carbon nanostructure, the TM-carbon binding takes

place through a charge-transfer mechanism and the TM remains in the cationic state. Therefore, the gas molecule can get absorbed on the cationic transition metal element giving some electronic charge [10–13].

The Silicon Carbide (SiC) monolayer as a new graphene-like semiconductor is a direct band gap material, while silicon being in the same group with the carbon represents attributes entirely analogous to that of carbon and makes it possible to generate powerful applications in optoelectronic and electronic instruments [14–19]. As the polarizability of Si is more than C, so it is expected that, due to stronger van der Waal's interaction, SiC/Si nano surface can bind compounds more strongly compared to

the pure carbon nanostructures. It is known that for optimum adsorption of gas molecules, the ideal form of binding between the host material (SiC nanosheet) and adsorbed gas molecules should be intermediate between physisorption and chemisorption energy [20].

In addition, transition metal (TM) atoms are considered to be the source of magnetism; in the results of TM-doped SiC monolayer, it can be found that the system can be a magnetic semiconductor by Co, Cu, Fe, Mn, and Ni doping [21]. The TM dopants can cause a total Hamiltonian perturbation, eventually leading to changes in electronic structures, which makes it a substantial application in magnetic electronic devices [22–28].

In this work, we shall present the theoretical estimates for the charge transfer and the energy of binding with the SiC surface for adsorption of molecules. Let us note that there also exist some model approaches to the problem of adsorption in addition to the popular and currently widely used first-

principles calculations. Then, it has been investigated the magnetic and electronic structures of Mn-doped graphene-like SiC sheet through adsorption of CO, CO₂, NO, NO₂ gas molecules (GM@ Mn–SiC_sh) by using first-principle calculations based on the density functional theory (DFT) [29]. The calculation is realized by generalized gradient approximation (GGA) potential and Perdew-Burke-Ernzerhof (PBE) functional [30,31].

THEORETICAL CONCEPTION, MATERIAL AND METHODS

For the SiC graphene-like sheet calculation the sheet has been modeled by alternatively arranged 15 C and 15 Si atoms. In a previous theoretical calculation, it is reported that the most stable structure of planar SiC forms graphene-like structure with alternative SiC bond and the bonding in such structure is of sp² type (Figure1) [32]. In our calculation we have considered similar structure and optimized without any symmetry constraint.

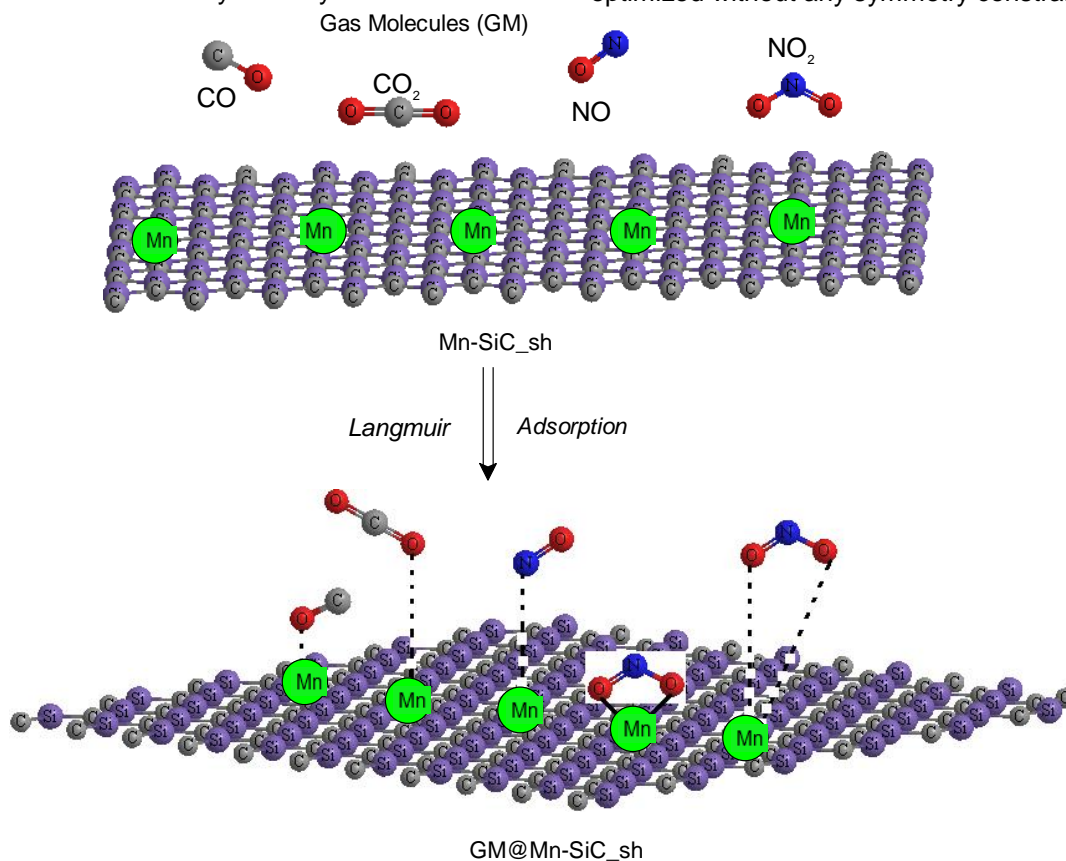


Figure 1. Langmuir adsorption of CO, CO₂, NO, and NO₂ onto Mn –doped SiC nanosheet.

The adsorbing of CO, CO₂, NO, NO₂ gas molecules on the surface of Mn –SiC_{sh} was defined by the theory Langmuir isotherm [33, 34], which indicates the chemisorption between gas molecules and Mn –SiC_{sh}. The

adsorbates of CO, CO₂, NO, NO₂ gas molecules are maintained on surface of Mn –SiC_{sh} with "Langmuir" chemisorption (Figure1).

In this research, the simulated calculations have been directed in the GaussView 6.06.16 [35] and calculated by Gaussian 16, Revision C.01 [36] using the DFT method. The [Perdew–Burke–Ernzerhof] (PBE) functional with high-precision generalized gradient approximation "GGA" has been employed to achieve more authentic results [37].

The binding energy is calculated as: $E_b = (E_t - 15E_{Si} - 15E_C)/30$, where E_t is the total energy after optimization, E_{Si} and E_C are the correction factors for Si and C atoms, respectively.

From the charge density distribution of the SiC sheet, it is seen that a considerable amount of electronic charge is transferred from Si to C site. The presence of these point charges on the SiC sheet influences the gas adsorption property.

After organizing the structure and energetics of SiC sheet, we have tried to decorate the sheet by manganese atom. A full geometry optimization has been done and the data has explored that that the most stable location of manganese is on the top of Si atom by pushing it down the surface.

Figure1 has shown that the SiC sheet is distorted from planarity after adding the manganese in such a way that the doped manganese can bind with Si atom along with three neighboring carbon atoms, therefore developing the stability of the system. When the manganese atom is on the silicon atom, the Mn–Si bond distance is 2.56 Å while Mn–C bond distance is 1.98 Å. After doping of manganese on the silicon atom, the planarity of the system is perturbed because silicon atom goes toward the sp^3 hybridization. Although silicon and carbon atoms are iso-valent, the most stable state of carbon is sp^2 and silicon is sp^3 . Then, we have tailored the spin-polarized DFT calculation with ONIOM model [38] accompanying the same force and energy convergence accuracy to the adsorption systems, with CAM-B3LYP [69] functional and with 6-311+G (d, p) [39] basis set for carbon, nitrogen, oxygen, silicon and LANL2DZ for manganese in the adsorption sites for the first layer (high level). Second layer (medium level) has been considered on some manganese atoms, carbon, and silicon atoms of SiC_{sh}, respectively, in the adsorption site due to semi-empirical methods. The third layer (low level) has been saved on the remained carbon and silicon atoms of SiC_{sh} with molecular mechanic force fields (Figure1) [38] as formula:

$$E_{\text{ONIOM}} = E_{1\text{st}} + E_{2\text{nd}} + E_{3\text{rd}} \quad (1)$$

It has been studied the interaction of CO, CO₂, NO, and NO₂ gas molecules with the Mn-decorated SiC sheet. The optimized geometries of the GM@ Mn-decorated SiC sheet are shown in Figure1.

The charge transfer between adsorbates of CO, CO₂, NO, NO₂ and adsorbent of Mn–SiC_{sh} is calculated due to the Bader charge analysis [40]. This method can measure charge accumulation from the charge of each atom in the complex model. Finally, the total adsorption charge transfer can be obtained as formula: $\Delta Q_t = Q_2 - Q_1$, where Q_2 and Q_1 remark the charge of CO, CO₂, NO, NO₂ after and before adoption, respectively. In fact, negative ΔQ_t indicates that electrons are transferred from gas molecules of CO, CO₂, NO, NO₂ to the surface of Mn–SiC_{sh}, and the adsorbent acts as an electron acceptor [41, 42].

The changes of charge density analysis in the adsorption process has illustrated that Mn–SiC_{sh} shows the Bader charge of –1.445e, before adsorption of CO, CO₂, NO, NO₂, and –2.072e, –1.371e, –1.331e, –1.342e after adsorption of CO, CO₂, NO, NO₂, respectively. Therefore, the changes of charge density for Langmuir adsorption of CO, CO₂, NO, NO₂ on Mn–SiC_{sh} surface alternatively are $> \Delta Q_{\text{NO} \rightarrow \text{Mn-SiC}} = +0.114e > \Delta Q_{\text{NO}_2 \rightarrow \text{Mn-SiC}} = +0.103e > \Delta Q_{\text{CO}_2 \rightarrow \text{Mn-SiC}} = +0.074e > \Delta Q_{\text{CO} \rightarrow \text{Mn-SiC}} = -0.627e$. The values of changes of charge density have shown a more important charge transfer for Mn–SiC_{sh} which acts as the electron acceptor while gas molecules act as the stronger electron donors through adsorption on the Mn–SiC_{sh} surface.

To determine the most sensitive structure of Mn–SiC_{sh} as the selective sensor for detecting gas molecules of CO, CO₂, NO, and NO₂, the binding energy of each system has been calculated. Therefore, we have found that the priority for selecting the surface binding of N-atom of NO, and O-atom of NO₂, CO, CO₂, in adsorption site can be impacted by the existence of close atoms in the Mn–SiC_{sh} surface. The simulated distribution functions of NO → Mn–SiC_{sh}, NO₂ → Mn–SiC_{sh}, CO → Mn–SiC_{sh}, and CO₂ → Mn–SiC_{sh} have illustrated that the created clusters lead to the bond lengths of N → Mn in NO → Mn–SiC_{sh} (2.07Å), O → Mn in NO₂ → Mn–SiC_{sh} (2.06Å), O → Mn in CO → Mn–SiC_{sh} (2.05Å) and O → Mn in CO₂ → Mn–SiC_{sh} (2.05Å) (Figure1).

RESULTS AND DISCUSSION

Electronic properties

The electronic structures of CO, CO₂, NO and NO₂ adsorbed on the Mn-doped SiC nanosheet (GM@ Mn–SiC_sh) have been analyzed to simplify subsequent discussion for interfacial electronic properties using CAM-B3LYP/ LANL2DZ, 6-311+G (d,p) basis sets.

Figure 2 shows the projected density of state (PDOS) of the Mn decorated SiC sheet. The appearance of the energy states (*d*-orbital) of Mn within the gap of SiC sheet induces the reactivity of the system. It is clear from the figure that after doping with Mn atom and there is a significant contribution of Mn *d*-orbital in

the unoccupied level. Based on the population analysis and DOS it can be concluded that Mn remains in the cationic state and it can accept more electrons from other atoms. Therefore, the graph of partial DOS (PDOS) has illustrated that the *p* states of the adsorption of N- and O- on the Mn –SiC_sh are dominant through the conduction band (Figure 2). A distinct metallic feature can be observed in SiC_sh because of the strong interaction between the *p* states of C, N, O, Si and the *d* state of Mn near the Fermi energy. Moreover, the existence of covalent features for these complexes has exhibited the identical energy amount and figure of the PDOS for the *p* orbitals of C, N, O, Si and *d* orbitals of Mn (Figure 2a-d).

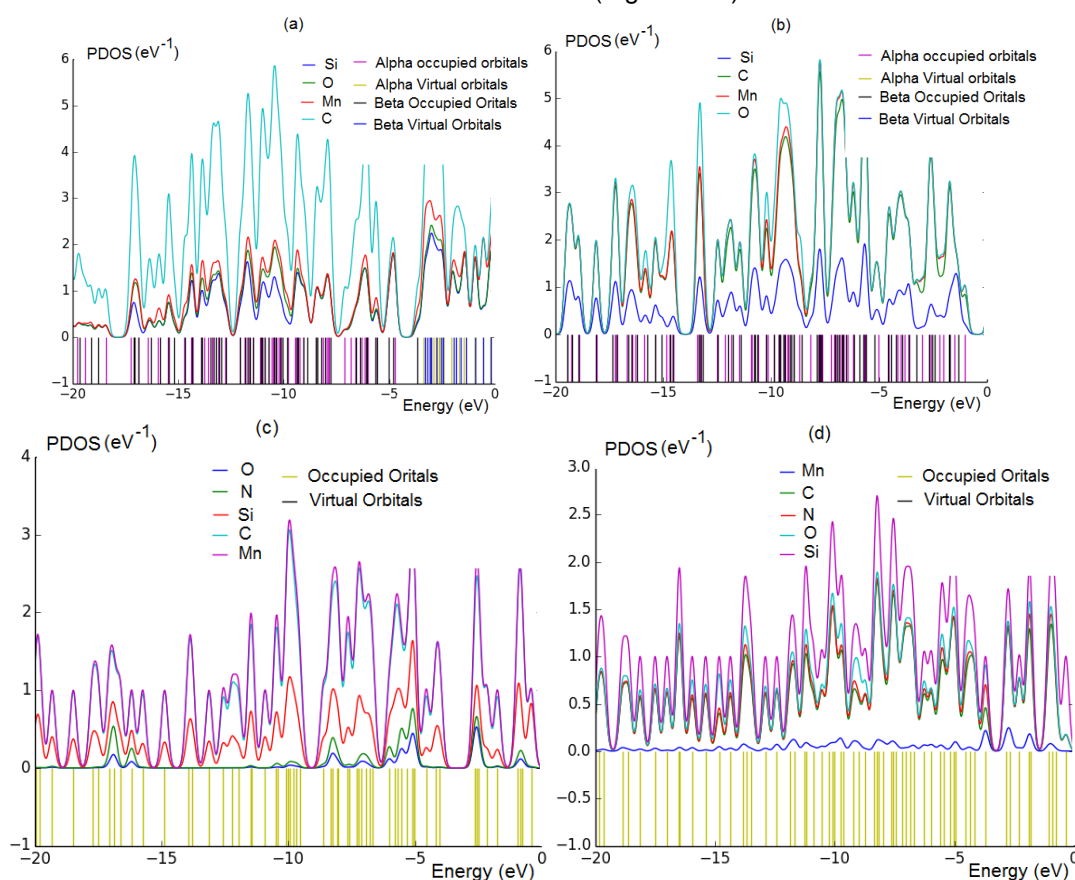


Figure 2. PDOS adsorption of a) CO@ Mn–SiC_sh, b) CO₂@ Mn–SiC, c) NO@ Mn–SiC, and d) NO₂@ Mn–SiC.

Figure 2 a,b shows that the CO and CO₂ states, respectively, onto Mn–SiC_sh have more contribution at the middle of the conduction band between –5eV to –10eV, while contribution of carbon and silicon states are expanded and close together, but manganese states have minor contributions.

Figure 2 c,d shows that the NO and NO₂ states, respectively, onto Mn –SiC_sh have more contribution at the middle of the

conduction band between –5eV to –10eV, while contribution of carbon and silicon states are expanded and close together, but manganese states have major contributions.

The results also approved by the partial electron density (PDOS) which have showed a certain charge association between Mn – SiC_sh and gas molecules of CO, CO₂, NO and NO₂.

Therefore, the above results exhibit that the cluster dominant of non-metallic and metallic features and a certain degree of covalent features can illustrate the increasing of the semiconducting direct band gap of gas molecules of CO, CO₂, NO and NO₂ adsorbing on Mn–SiC_{sh}.

Nuclear quadrupole resonance (NQR) analysis

NQR procedure has been done out for the complexes of gas molecules of CO, CO₂, NO and NO₂ adsorbing on Mn–SiC_{sh} [43–46]. Since the electric field gradient at the situation of CO, CO₂, NO and NO₂ adsorbed on the Mn–SiC_{sh} surface as the gas detector is approved by the valence electrons distorted in the special connection with close nuclei of Mn-doped SiC nanosheet, the nuclear quadrupole resonance at which transitions occur is special for NO@ Mn–SiC_{sh} and NO₂@ Mn–SiC_{sh} (Table1).

Table 1. The electric potential (E_p) and Bader charge (Q) for elements involving in the adsorption mechanism of CO, CO₂, NO and NO₂ adsorbed on the Mn-doped SiC nanosheet using CAM–B3LYP/EPR–III, 6-311+G (d,p) calculation extracted of NQR method.

CO@Mn–SiC _{sh}			CO ₂ @Mn–SiC _{sh}			NO@Mn–SiC _{sh}			NO ₂ @Mn–SiC _{sh}		
Atom	Q	E_p	Atom	Q	E_p	Atom	Q	E_p	Atom	Q	E_p
C1	0.1739	–14.5306	C1	0.3878	–14.3091	O1	–0.1238	–22.0713	N1	–0.2068	–18.1293
O2	–0.4342	–22.099	O2	–0.1744	–21.7965	N2	–0.2289	–18.1784	O2	–0.1823	–21.814
C3	–0.9409	–14.7719	C3	–0.8427	–14.8316	C3	–0.8471	–14.8329	O3	–0.2046	–22.0061
Si4	0.9855	–49.0393	Si4	0.8072	–48.6328	Si4	0.8281	–48.6201	C4	–0.8298	–14.8164
C5	–0.8978	–14.7804	C5	–0.8304	–14.8296	C5	–0.8240	–14.8266	Si5	0.8352	–48.6115
Si6	1.3409	–49.0426	Si6	1.1254	–48.573	Si6	1.1517	–48.5675	C6	–0.8272	–14.8274
C7	–0.8561	–14.8117	C7	–0.8218	–14.8701	C7	–0.8194	–14.8758	Si7	1.2123	–48.5338
C8	–1.6613	–14.7618	C8	–1.2347	–14.8183	C8	–1.1912	–14.8019	C8	–0.8368	–14.8791
Si9	1.4326	–49.0446	Si9	1.1557	–48.572	Si9	1.1717	–48.5694	C9	–1.1446	–14.7803
Si10	1.4459	–49.0432	Si10	1.1755	–48.5698	Si10	1.1764	–48.5706	Si10	1.1509	–48.568
C11	–0.9395	–14.7703	C11	–0.8430	–14.8301	C11	–0.8379	–14.8257	Si11	1.1913	–48.5544
C12	–1.9750	–14.8015	C12	–1.2009	–14.8075	C12	–1.2000	–14.7911	C12	–0.8404	–14.8192
Si13	1.1412	–49.0196	Si13	0.8393	–48.6246	Si13	0.8466	–48.6186	C13	–1.1992	–14.7933
Si14	2.0720	–48.9766	Si14	1.2450	–48.5298	Si14	1.3313	–48.4864	Si14	0.8478	–48.6203
C15	–1.6537	–14.7572	C15	–1.2330	–14.8219	C15	–1.1967	–14.7893	Si15	1.3423	–48.476
C16	–1.6360	–14.7564	C16	–1.2294	–14.8169	C16	–1.1889	–14.786	C16	–1.0606	–14.6896
Mn17	1.4512	–108.73	Mn17	1.3708	–107.877	Mn17	1.3196	–107.82	C17	–1.1797	–14.7998
Si18	1.4015	–49.0392	Si18	1.1490	–48.5718	Si18	1.1540	–48.5705	Mn18	1.3220	–107.852
C19	–0.8701	–14.8122	C19	–0.8253	–14.8749	C19	–0.8179	–14.8781	Si19	1.1691	–48.5671
C20	–1.9392	–14.8091	C20	–1.2230	–14.8187	C20	–1.2184	–14.767	C20	–0.8188	–14.8718
Si21	1.2706	–49.0054	Si21	0.8050	–48.6576	Si21	0.7597	–48.6627	C21	–1.2179	–14.7695
Si22	1.9429	–48.9851	Si22	1.2938	–48.5367	Si22	1.3172	–48.4959	Si22	0.7550	–48.668
C23	–1.9485	–14.8105	C23	–1.2467	–14.8375	C23	–1.2530	–14.8096	Si23	1.3210	–48.4957
C24	–1.9901	–14.775	C24	–1.2035	–14.8056	C24	–1.1975	–14.7932	C24	–1.2472	–14.8039
Si25	2.0466	–48.973	Si25	1.2739	–48.5211	Si25	1.3289	–48.4877	C25	–1.1989	–14.7988
Si26	1.1514	–49.0083	Si26	0.8420	–48.622	Si26	0.8415	–48.6238	Si26	1.3054	–48.5013
C27	–0.8985	–14.7648	C27	–0.8280	–14.8261	C27	–0.8218	–14.8308	Si27	0.8467	–48.623
C28	–0.9721	–14.7416	C28	–0.8888	–14.8566	C28	–0.8493	–14.7746	C28	–0.8294	–14.8323
Si29	1.1916	–48.9756	Si29	0.8418	–48.6387	Si29	0.9248	–48.5729	C29	–0.8493	–14.7778
Si30	1.0521	–48.9901	Si30	0.8337	–48.6419	Si30	0.9209	–48.5767	Si30	0.9198	–48.5783
C31	–1.9532	–14.8041	C31	–1.2232	–14.8188	C31	–1.2188	–14.7677	Si31	0.9174	–48.5799
Si32	1.4660	–48.9735	Si32	0.8203	–48.6499	Si32	0.7612	–48.6645	C32	–1.2181	–14.7698
			O33	–0.1176	–21.8077				Si33	0.7554	–48.6693

Furthermore, in Figure3 (a-d) it has been drawn the electric potential of nuclear quadrupole resonance method versus Bader charge for elements of carbon, nitrogen, oxygen, silicon and manganese in the adsorption process of CO, CO₂, NO and NO₂

on the Mn-doped SiC nanosheet by CAM–B3LYP/EPR–III, 6-311+G (d,p), LANL2DZ theoretical level. It has been remarked the changes of electric potential for carbon, nitrogen, oxygen, silicon and manganese in the active site of Langmuir adsorption.

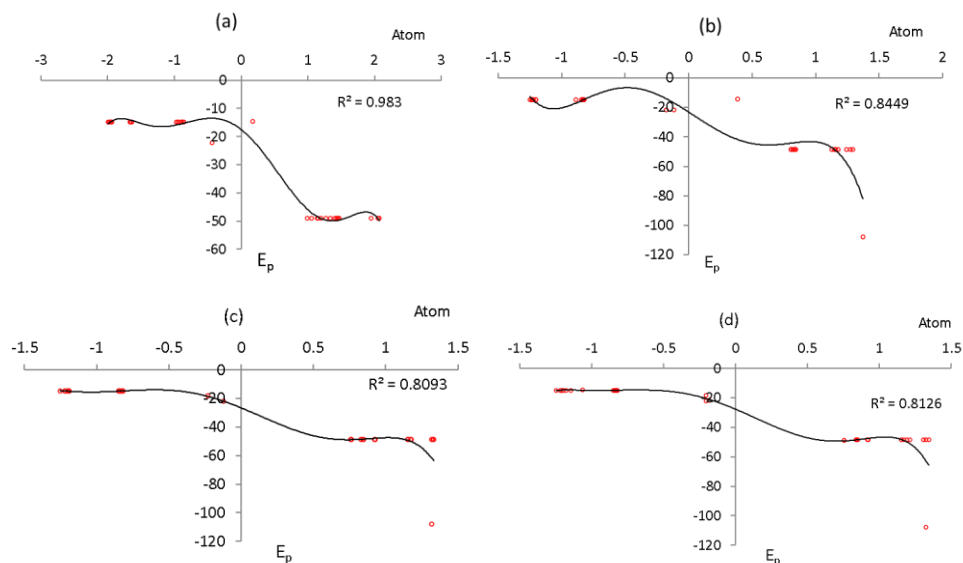


Figure 3. The electric potential (E_p) versus Bader charge (Q) for elements involving in the adsorption mechanism of CO, CO₂, NO and NO₂ adsorbed on the Mn-doped SiC nanosheet.

In fact, it has been observed the effect of the binding between C, N and O atoms of gas molecules with manganese doping in the SiC nanosheet during adsorbing CO, CO₂, NO and NO₂ through resulted electric potential using NQR analysis (Figure3a-d). It's obvious that the capability of SiC nanosheet for detecting of CO, CO₂, NO and NO₂ is fluctuated by their selectivity and sensitivity which can represent the efficiency of these surfaces as the promising sensors (Figure3a-d).

Magnetism of gas adsorption onto Mn - Doped SiC Monolayer

Isotropic (σ_{iso}) and anisotropy (σ_{aniso}) shielding tensors of NMR spectroscopy for certain atoms in the active site of CO, CO₂, NO and NO₂ adsorbed on the Mn-doped SiC nanosheet (GM @ Mn -SiC_{sh}) through the formation of the binding between gas molecules and solid surfaces have been calculated using Gaussian 16, Revision C.01 and reported in Tables2 [36].

Table2. Data of GIAO/NMR shielding tensors for selected atoms of CO, CO₂, NO and NO₂ adsorbed on the Mn-doped SiC nanosheet (GM@ Mn -SiC_{sh}) using CAM-B3LYP/EPR-III, 6-311+G (d,p) calculation.

CO@ Mn-SiC _{sh}			CO ₂ @ Mn-SiC _{sh}			NO@ Mn-SiC _{sh}			NO ₂ @ Mn-SiC _{sh}		
Atom	σ_{iso}	σ_{aniso}	Atom	σ_{iso}	σ_{aniso}	Atom	σ_{iso}	σ_{aniso}	Atom	σ_{iso}	σ_{aniso}
C1	839.3946	1002.2788	C1	96.1400	93.1721	O1	4955.9720	16266.0801	N1	6.9507	377.3925
O2	276.2067	874.7320	O2	330.6883	232.7966	N2	2921.6143	9508.9334	O2	447.7076	734.5976
C3	69.3693	276.6091	C3	103.2194	284.3349	C3	63.8247	316.5862	O3	306.6233	649.2107
Si4	390.2435	400.5878	Si4	369.3930	411.8930	Si4	342.3272	752.6769	C4	101.9741	665.3349
C5	21.8365	397.8211	C5	29.3183	427.8886	C5	67.8482	547.0680	Si5	544.0870	416.6760
Si6	464.6136	464.6136	Si6	538.1384	200.6927	Si6	547.0680	529.0565	C6	99.4095	557.3271
C7	34.3820	156.6012	C7	3.8675	246.2114	C7	468.2217	1277.4161	Si7	585.8655	211.7964
C8	3.2502	160.4014	C8	124.7322	206.1069	C8	283.8816	455.1895	C8	238.0006	673.8098
Si9	449.5127	231.8515	Si9	498.6096	190.9195	Si9	489.0228	189.6011	C9	135.6258	443.7472
Si10	436.0893	233.7164	Si10	498.5525	224.2899	Si10	461.2910	580.6822	Si10	555.1295	398.8867
C11	56.6421	245.3379	C11	92.2521	280.2964	C11	102.5761	795.5452	Si11	561.1546	357.4789
C12	137.7832	129.2250	C12	183.6525	138.3295	C12	148.0671	197.1164	C12	212.2994	435.3873
Si13	331.9986	449.7336	Si13	331.7981	619.3365	Si13	220.8788	852.9392	C13	159.9865	213.5473
Si14	503.0099	116.3529	Si14	535.7653	169.3535	Si14	587.1419	332.5067	Si14	289.5950	768.4587
C15	36.6687	132.7677	C15	120.0345	104.3311	C15	164.1976	302.4012	Si15	548.5386	233.2020
C16	24.3139	156.3795	C16	101.4652	143.5871	C16	126.2236	324.8641	C16	165.0720	31.9988
Mn17	5490.0662	5490.0662	Mn17	577.2588	4720.9986	Mn17	2253.4161	3427.6443	C17	74.5809	115.9314
Si18	480.5459	225.2728	Si18	523.3562	244.9164	Si18	472.8409	395.0810	Mn18	3065.8978	2407.8324
C19	20.3862	202.4985	C19	25.8686	195.2969	C19	675.3813	2140.5004	Si19	607.4191	227.8249
C20	19.5751	260.6555	C20	84.1860	231.8100	C20	128.2984	238.4227	C20	214.8667	549.5050
Si21	487.7266	789.1558	Si21	268.9918	1044.4687	Si21	30.0117	1438.8372	C21	84.1405	308.0750
Si22	509.1258	146.0888	Si22	490.1955	212.9274	Si22	535.9755	347.0423	Si22	251.5197	1407.6778
C23	170.5696	83.7421	C23	236.0804	129.2938	C23	220.6460	130.0343	Si23	535.5484	375.4029

CO@ Mn–SiC_sh			CO ₂ @ Mn–SiC_sh			NO@ Mn–SiC_sh			NO ₂ @ Mn–SiC_sh		
Atom	σ_{iso}	σ_{aniso}	Atom	σ_{iso}	σ_{aniso}	Atom	σ_{iso}	σ_{aniso}	Atom	σ_{iso}	σ_{aniso}
C24	167.7952	96.3575	C24	191.4252	127.5715	C24	180.8217	155.5782	C24	228.2656	151.8448
Si25	514.9060	190.2335	Si25	528.6962	145.4086	Si25	535.2125	355.0449	C25	170.1081	164.6837
Si26	345.4313	475.6214	Si26	311.0367	631.6643	Si26	180.3473	919.8871	Si26	579.9495	392.4220
C27	62.8710	431.8817	C27	36.9630	435.3123	C27	123.5446	650.0646	Si27	282.4011	773.8116
C28	62.9182	357.3340	C28	4.4398	219.0559	C28	16.2414	279.6840	C28	103.2243	562.2834
Si29	435.5945	320.4293	Si29	363.2361	267.7715	Si29	332.6151	449.8710	C29	46.5832	128.1382
Si30	372.2834	130.5793	Si30	349.0169	311.4886	Si30	384.2394	448.8511	Si30	465.3427	436.7001
C31	51.9143	152.9209	C31	83.9874	231.0541	C31	94.0863	309.2761	Si31	447.8803	460.5937
Si32	470.4142	478.8400	Si32	318.4667	946.0263	Si32	90.2641	1652.7068	C32	87.2781	296.3040
			O33	136.1346	174.3622				Si33	193.5788	1396.4866

"Isotropic chemical-shielding" (σ_{iso}) & "anisotropic chemical-shielding" (σ_{aniso}) [47]: $\sigma_{iso} = \frac{\sigma_{33} + \sigma_{22} + \sigma_{11}}{3}$; $\sigma_{aniso} = \sigma_{33} - \frac{\sigma_{22} + \sigma_{11}}{2}$

The resulted of NMR data in Table2 have shown approximately the identical chemical shielding behavior of isotropic and anisotropy factors of GM @ Mn–SiC_sh with several sharp peaks related to carbon, nitrogen, oxygen, silicon and manganese of gas molecules (adsorbate) and TM-doped SiC nanosheet (adsorbent) in the active site situations (Figure 4). CO@ Mn–SiC_sh with a

sharp peak related to the adsorption site for atom of Mn17 (Figure4a); CO₂@ Mn–SiC_sh with a sharp peak for atom of Mn 17 (Figure4b); NO@ Mn –SiC_sh with several sharp peaks for atoms of O1 and a minor peak for atom of Mn 17 (Figure4c); and NO₂@ Mn –SiC_sh with a sharp peak for atom of Mn18 have been indicated (Figure4d).

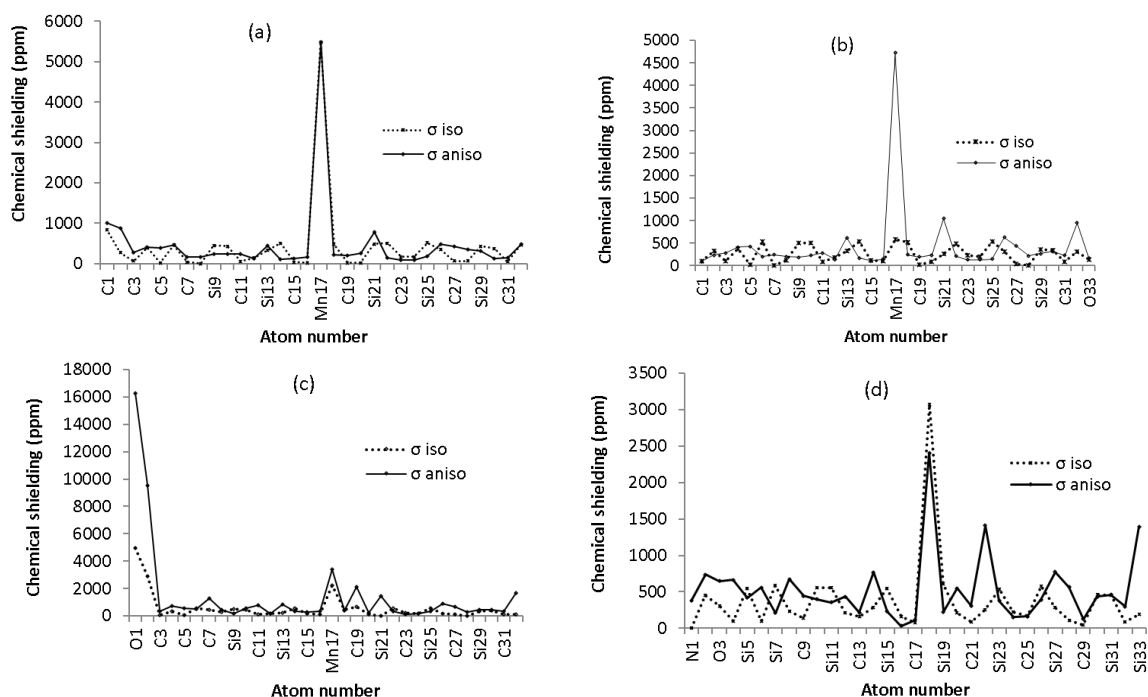


Figure 4. NMR adsorbing of CO, CO₂, NO and NO₂ on the Mn–doped SiC nanosheet through production of clusters of a) CO@ Mn–SiC_sh, b) CO₂@ Mn–SiC_sh c) NO@ Mn–SiC_sh, and d) NO₂@ Mn–SiC_sh by CAM–B3LYP/EPR–III, LANL2DZ,6-31+G(d,p).

Although, in the NMR spectroscopy, it has been observed the remarkable peaks around silicon and manganese atoms in the SiC nanosheets through the adsorption procedure of gas molecules, there are some fluctuations in the chemical shielding behaviors of isotropic and anisotropy attributes.

Vibrations of gas adsorption onto Mn - Doped SiC Monolayer

In this part, the stability of complexes including gas adsorption on manganese (Mn) metal-doped graphene-like silicon carbide (SiC) monolayer sheet has been investigated through thermodynamic properties which define the reactions that CO, CO₂, NO, and NO₂ endure in the Mn –SiC_sh coordination sphere. Concerning adsorption process, the thermodynamic characters were evaluated for CO, CO₂, NO, and NO₂ on the surface of Mn–

SiC_sh as the gas detectors which can be applicable as the selective sensors for these

gases (Table3).

Table 3. The thermodynamic character of CO, CO₂, NO, and NO₂ adsorbed on the Mn–SiC_sh as the selective gas sensors

Compound	$\Delta E^{\circ} \times 10^{-4}$ (kcal/mol)	$\Delta H^{\circ} \times 10^{-4}$ (kcal/mol)	$\Delta G^{\circ} \times 10^{-4}$ (kcal/mol)	S° (Cal/K.mol)	Dipole moment (Debye)
CO	-6.9784	-6.9784	-6.9798	47.100	0.2373
CO ₂	-11.6121	-11.6121	-11.6136	51.378	0.0000
NO	-8.0017	-8.0016	-8.0031	48.968	0.2376
NO ₂	-12.6298	-12.6298	-12.6315	57.792	0.2323
SiC_sh	-304.3389	-304.3389	-304.3417	93.684	9.6011
Mn –SiC_sh	-453.612	-453.611	-453.639	95.316	4.6774
CO@ Mn –SiC_sh	-367.1664	-367.1663	-367.1692	98.807	5.2228
CO ₂ @ Mn –SiC_sh	-369.5081	-369.5080	-369.5111	104.352	5.0810
NO@ Mn –SiC_sh	-365.8765	-365.8764	-365.8793	96.939	11.6623
NO ₂ @ Mn –SiC_sh	-370.5016	-370.5015	-370.5044	95.454	10.5278

Furthermore, the IR spectrums for adsorption of CO, CO₂, NO, and NO₂ on the surfaces of Mn–SiC_sh have been reported in Figure5 (a-d). The graph of Figure5 (a) has been observed in the frequency range between 1000–2500 cm⁻¹ for the complex of CO@Mn–SiC_sh with several sharp peaks around 1900 – 2500 cm⁻¹.

Figure5 (b) has shown the graph of IR peaks for CO₂@ Mn–SiC_sh approximately between

1500 cm⁻¹–3000 cm⁻¹ with several sharp peaks around 1600–1800cm⁻¹. Figure5 (c) has shown the graph of IR peaks for NO@ Mn –SiC_sh approximately between 700–2500 cm⁻¹ with several considerable peaks around 2000–2300cm⁻¹. Figure5 (d) has exhibited the graph of IR peaks for NO₂@ Mn –SiC_sh approximately between 700–2500 cm⁻¹ with several sharp peaks around 2200–2400 cm⁻¹.

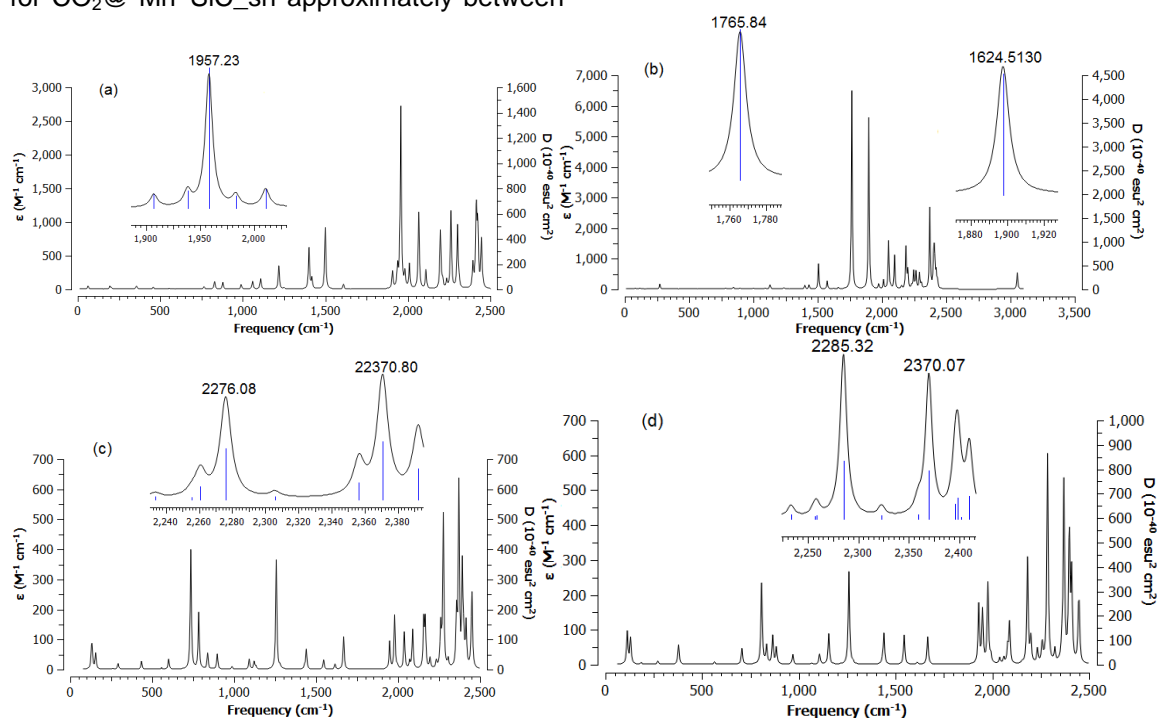


Figure 5. The Frequency (cm-1) changes through the "IR" spectrums for a) CO@ Mn –SiC_sh, b) CO₂@ Mn –SiC_sh, c) NO@ Mn –SiC_sh and d) NO₂@ Mn –SiC_sh as the selective gas detectors.

The adsorptive capacity of CO, CO₂, NO, and NO₂ on the surface of Mn –SiC_sh is approved by the ΔE°_{ads} amounts as formula:

$$\Delta E^{\circ}_{ads} = \Delta E^{\circ}_{X \rightarrow Mn-SiC_{sh}} - (\Delta E^{\circ}_X + \Delta E^{\circ}_{Mn-SiC_{sh}});$$

$$(X=CO, CO_2, NO, NO_2) \quad (2)$$

Table3 has shown that the adsorbing of CO, CO₂, NO, and NO₂ on the surface of Mn –

SiC_sh must have both "physical" and "chemical" nature. All the measured relative adsorption energies ($\Delta E_{\text{ads}}^{\circ}$) are almost identical, and exhibit the accord of the estimated data by all methods and the accuracy of the calculations. In fact, Mn – SiC_sh has higher interaction energy from Van der Waals' forces with gas molecules including CO, CO₂, NO, and NO₂ that can make them highly stable.

Furthermore, the difference of ΔH_R among adsorption of CO, CO₂, NO, and NO₂ on the surface of Mn –doped SiC_sh has been unraveled due to non-covalent binding resulted from interatomic interactions between gas molecules and surface (GM@ Mn –SiC) and covalent binding resulted from intra-atomic interactions between transition metal of manganese and silicon carbide nanosheet (Mn –SiC_sh) (Table3).

For the adsorption mechanism, $\Delta G_{\text{ads}}^{\circ}$ is calculated as follows:

$$\Delta G_{\text{ads}}^{\circ} = \Delta G_{\text{X} \rightarrow \text{Mn-SiC_sh}}^{\circ} - (\Delta G_{\text{X}}^{\circ} + \Delta G_{\text{Mn-SiC_sh}}^{\circ});$$

$$(X = \text{CO}, \text{CO}_2, \text{NO}, \text{NO}_2) \quad (3)$$

On the basis of data in Table3, it is predicted that the adsorption of the gas molecules on the Mn –SiC_sh surface might be physical and chemical nature. As shown in Table3, all the computed $\Delta G_{\text{ads}}^{\circ}$ amounts are close, which exhibits the accord of the evaluated data by all methods and the validity of the computations.

However, Mn –SiC_sh surface seems possess enough efficiency for adsorption of gas molecules containing CO, CO₂, NO, and NO₂ through charge transfer from nitrogen and oxygen to the manganese element doping of silicon carbide due to intra-atomic and interatomic interactions.

Furthermore, the difference of ΔH_R among adsorption of CO, CO₂, NO, and NO₂ on the surface of Mn–doped SiC_sh has been unraveled due to non-covalent binding resulted from interatomic interactions between

gas molecules and surface (GM@Mn–SiC) and covalent binding resulted from intra-atomic interactions between transition metal of manganese and silicon carbide nanosheet (Mn–SiC_sh) (Figure6).

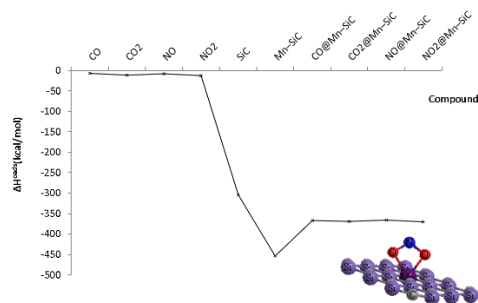


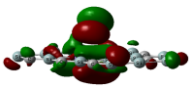
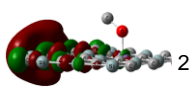
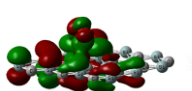
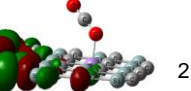
Figure 6. The alterations of relative adsorption energy ($\Delta H_{\text{ads}}/\text{kcal.mol}^{-1}$) for the reaction of CO, CO₂, NO, and NO₂ adsorbed on the surface of Mn–SiC_sh.

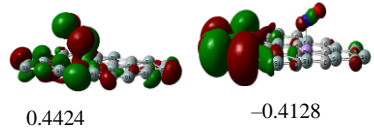
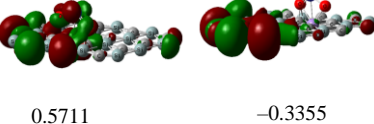
Figure6 has indicated the heat of formation ($\Delta H_{\text{ads}}^{\circ}$) between initial compounds of CO, CO₂, NO, NO₂, surface of SiC_sh, Mn–doped SiC_sh nanosheet and product compounds of CO@ Mn–SiC_sh, CO₂@ Mn–SiC_sh, NO@ Mn–SiC_sh and NO₂@ Mn–Si_sh.

Analysis of HOMO & LUMO

Based on frontier molecular orbital FMO theory, the LUMO and HOMO and the energy between them is the band gap of the adsorption system were computed. In fact, broad band gap diagram indicates that there is less conductivity [48-50]. The LUMO, HOMO, band energy gap (ΔE) and other quantities distributions of CO, CO₂, NO, and NO₂ on the surfaces of Mn –SiC_sh as the gas detector systems denote that the gas adsorption procedure scatters the electrons of the system (Table 4).

Table 4. LUMO (eV), HOMO (eV), band energy gap (ΔE /eV) and other quantities (eV) distributions of CO, CO₂, NO, and NO₂ on the surfaces of Mn –SiC_sh.

Gas → Mn–SiC_sh	LUMO	HOMO	ΔE	μ	χ	η	ζ	ψ
CO@ Mn–SiC_sh	 -3.3303	 -5.6297	2.2994	-4.48	4.48	1.1497	0.4350	8.7285
CO ₂ @ Mn–SiC_sh	 1.2612	 -1.0046	2.2658	0.1283	-0.1283	1.1329	0.4413	0.0072

NO@ Mn –SiC_sh		0.8552	0.0148	-0.0148	0.4276	1.1693	2.5612
NO ₂ @ Mn –SiC_sh		0.9066	0.1178	-0.1178	0.4533	1.1030	0.0153

Band energy gap: $\Delta E = E_{\text{LUMO}} - E_{\text{HOMO}}$; Chemical potential: $\mu = (E_{\text{HOMO}} + E_{\text{LUMO}})/2$; Electronegativity: $\chi = -(E_{\text{HOMO}} + E_{\text{LUMO}})/2$; Hardness: $\eta = (E_{\text{LUMO}} - E_{\text{HOMO}})/2$; Softness: $\zeta = 1/(2\eta)$; electrophilicity index: $\psi = \mu^2/(2\eta)$ [49,50].

The energy gap between HOMO and LUMO has represented the transporting of molecular electrical characters [51]. On the other hand, the difference between HOMO and LUMO has exhibited that the effect of the adsorption process on the electronic behavior of CO, CO₂, NO, and NO₂ on the surfaces of Mn –SiC_sh nanosheet (Table4). Other quantities (eV) consisting of Chemical potential, electronegativity, hardness, Softness, and electrophilicity index show an agreeable yield for capturing CO, CO₂, NO, and NO₂ by Mn –SiC_sh nanosheet (Table4).

The illustration of donor–acceptor molecules depends on the relative frontier molecular levels. The HOMO-LUMO gap defines the charge transfer in gas molecules adsorbed on the Mn–SiC_sh nanosheet through simplified molecular-level diagram. In fact, the amount of transferred charges might be considerably small, as in the case of parallel and perpendicular coordination, which indicate electronic couplings smaller than in co-facial coordination. The results in Table 4 have indicated the energy level shifts of gas molecule→surface-HOMO and gas molecule→surface-LUMO of nanoclusters as a function of their distance d orbitals from the high symmetry points of each gas molecule on the Mn–SiC_sh nanosheet. Therefore, the HOMO level of molecule is being lowered as it loses its electron, whereas the LUMO level of surface is being raised as it gains partial charge.

CONCLUSION

In summary, the nonmetal element-doped SiC nanosheet has been studied by first-principle calculations. Different dopants of gas molecules and doping sites are considered.

The current research wanted to remark the illustration of gas adsorption on Mn –SiC_sh nanosheet. Particularly, the structural, energetic, and infrared adsorption properties of

linearly "atop" for CO, CO₂, NO, and NO₂ gas molecules adsorbing on Mn –SiC_sh nanosheet has been explored by using DFT calculations.

The values of changes of charge density have shown a more important charge transfer for Mn –SiC_sh nanosheet which acts as the electron acceptor while gas molecules act as the stronger electron donors through adsorption on the Mn –SiC_sh nanosheet surface. It has been assumed that the priority for selecting the surface binding of N-atom of NO, and O-atom of NO₂, CO and CO₂ in adsorption site can be impacted by the existence of close atoms in the Mn –SiC_sh surface.

In fact, Mn site in SiC_sh nanosheet has higher interaction energy from Van der Waals' forces with gas molecules including CO, CO₂, NO, and NO₂ that can make them highly stable. Finally, our molecular simulation consequences have exhibited the existence of orbital hybridization between manganese site and gas molecules of CO, CO₂, NO, and NO₂ that also approves the recovery of adsorption susceptibility of graphene sheet. In fact, Mn –SiC_sh surface can promise an applicable outlook in the field of CO, CO₂, NO, and NO₂ gas sensor.

ACKNOWLEDGEMENTS

In successfully completing this paper and its research, the authors are grateful to Kastamonu University for their support through the office, library, and scientific websites.

REFERENCES

- [1] Novoselov, K.S., Geim, A.K., Morozov, S.V., Jiang, D., Zhang, Y., Dubonos, S.V., Grigorieva, I.V., Firsov, A.A.: Electric field effect in atomically thin carbon films. *Science* **306**, 666–669 (2004)

- [2] Geim, K.: Graphene: status and prospects. *Science* **324**, 1530–1534 (2009)
- [3] Castro Neto, A.H., Guinea, F., Peres, N.M.R., Novoselov, K.S., Geim, A.K.: The electronic properties of graphene. *Rev. Mod. Phys.* **81**, 109–162 (2009)
- [4] Mak, K.F., Lee, C., Hone, J., Shan, J., Heinz, T.F.: Atomically thin mos2: a new direct-gap semiconductor. *Phys. Rev. Lett.* **105**, 136805–136807 (2010)
- [5] Radisavljevic, B., Radenovic, A., Brivio, J., Giacometti, V., Kis, A.: Single-layer MoS2 transistors. *Nat. Nanotechnol.* **6**, 147–150 (2011)
- [6] Rodin, S., Carvalho, A., Castro Neto, A.H.: Strain-induced gap modification in black phosphorus. *Phys. Rev. Lett.* **112**, 176801–176803 (2014)
- [7] Low, T., Rodin, A.S., Carvalho, A., Jiang, Y., Wang, H., Xia, F., Castro Neto, A.H.: Tunable optical properties of multilayer black phosphorus thin films. *Phys. Rev. B* **90**, 075434–074538 (2014)
- [8] Fei, R., Faghaninia, A., Soklaski, R., Yan, J.A., Lo, C., Yang, L.: Enhanced thermoelectric efficiency via orthogonal electrical and thermal conductances in phosphorene. *Nano Lett.* **14**, 6393–6399 (2014).
- [9] Ramasubramaniam, A., Muniz, A.R.: Ab initio studies of thermodynamic and electronic properties of phosphorene nanoribbons. *Phys. Rev. B* **90**, 085424–085429 (2014)
- [10] Mollaamin, F.; Monajjemi, M. Doping of Graphene Nanostructure with Iron, Nickel and Zinc as Selective Detector for the Toxic Gas Removal: A Density Functional Theory Study. *C* **2023**, 9, 20. <https://doi.org/10.3390/c9010020>.
- [11] Ziqi Yan, Yu Bai and Lingjie Sun, Adsorption of thiophene and SO_x molecules on Cr-doped and Ti-doped graphene nanosheets: a DFT study. *Materials Research Express*, 6 (12), 2019. Doi: 10.1088/2053-1591/ab599d.
- [12] Mollaamin, F.; Monajjemi, M. Graphene Embedded with Transition Metals for Capturing Carbon Dioxide: Gas Detection Study Using QM Methods. *Clean Technol.* 2023, 5(1), 403–417. <https://doi.org/10.3390/cleantechnol5010020>.
- [13] Mollaamin, F., Monajjemi, M. Transition metal (X = Mn, Fe, Co, Ni, Cu, Zn)-doped graphene as gas sensor for CO₂ and NO₂ detection: a molecular modeling framework by DFT perspective. *J Mol Model* **29**, 119 (2023). <https://doi.org/10.1007/s00894-023-05526-3>.
- [14] Narushima, T., Goto, T., Hirai, T., Iguchi, Y.: High-temperature oxidation of silicon carbide and silicon nitride. *Mater. Trans. JIM* **38**, 821–835 (1997)
- [15] Zhang, X.H., Han, J.C., Zhou, J.G., Xin, C., Zhang, Z.H., Song, B.: Ferromagnetism in homogeneous (Al, Co)-codoped 4h-silicon carbides. *J. Magn. Magn. Mater.* **363**, 34–42 (2014)
- [16] Casady, J.B., Johnson, R.W.: Status of silicon carbide (SiC) as a wide-band gap semiconductor for high-temperature applications: a review. *Solid-St. Electron* **39**, 1409–1422 (1996).
- [17] Lin, S.S.: Light-emitting two-dimensional ultrathin silicon carbide. *J. Phys. Chem. C* **116**, 3951–3955 (2012) .
- [18] Hsueh, H.C., Guo, G.Y., Louie, S.G.: Excitonic effects in the optical properties of a SiC sheet and nanotubes. *Phys. Rev. B* **84**, 085404–085413 (2011)
- [19] Eliseeva, N.S., Kuzubov, A.A., Ovchinnikov, S.G., Serzhantova, M.V., Tomilin, F.N., Fedorov, A.S.: Theoretical study of the magnetic properties of ordered vacancies in 2D hexagonal structures: graphene, 2D-SiC, and H-BN. *JETP Lett.* **95**, 555–559 (2012)
- [20] Lee Hoonkyung, Ihm Jisoon, Marvin Cohen L, Louie Steven G. Calcium-decorated carbon nanotubes for high-capacity hydrogen storage: first-principles calculations. *Phys Rev B* 2009; 80:115412.
- [21] Bekaroglu, E., Topsakal, M., Cahagiurov, S., Ciraci, S.: Firstprinciples study of defects and adatoms in silicon carbide honeycomb structures. *Phys. Rev. B* **81**, 075433–075441 (2010)
- [22] Alaal, N., Loganathan, V., Medhekar, N., Shukla, A.: First principles many-body calculations of electronic structure and optical properties of SiC nanoribbons. *J. Phys. D: Appl. Phys.* **49**, 105306–105314 (2016)
- [23] Javan, M.B.: Electronic and magnetic properties of monolayer SiC sheet doped with 3d-transition metals. *J. Magn. Magn. Mater.* **401**, 656–661 (2016)
- [24] Wu, Y., Zhou, L.P., Du, X.Z., Yang, Y.P.: Near-field radiative heat transfer between two SiC plates with/without coated metal films. *J. Nanosci. Nanotechnol.* **15**, 3017–3024 (2015)

- [26] Bekaroglu, E., Topsakal, M., Cahagiurov, S., Ciraci, S.: Firstprinciples study of defects and adatoms in silicon carbide honeycomb structures. *Phys. Rev. B* **81**, 075433–075441 (2010)
- [27] Alaal, N., Loganathan, V., Medhekar, N., Shukla, A.: First principles many-body calculations of electronic structure and optical properties of SiC nanoribbons. *J. Phys. D: Appl. Phys.* **49**, 105306–105314 (2016)
- [28] Javan, M.B.: Electronic and magnetic properties of monolayer SiC sheet doped with 3d-transition metals. *J. Magn. Mater.* **401**, 656–661 (2016)
- [29] Wu, Y., Zhou, L.P., Du, X.Z., Yang, Y.P.: Near-field radiative heat transfer between two SiC plates with/without coated metal films. *J. Nanosci. Nanotechnol.* **15**, 3017–3024 (2015)
- [30] Kresse, G., Furthmüller, J.: Efficient iterative schemes for ab initio total-energy calculations using a plane-wave basis set. *Phys. Rev. B* **54**, 11169–11186 (1996)
- [31] Perdew, J.P., Burke, K., Ernzerhof, M.: Generalized gradient approximation made simple. *Phys. Rev. Lett.* **77**, 3865–3868 (1996)
- [32] Kresse, G., Joubert, D.: From ultrasoft pseudopotentials to the projector augmented-wave method. *Phys. Rev. B* **59**, 1758–1775 (1999)
- [33] Miyamoto Y, Yu BD. Computational designing of graphitic silicon carbide and its tubular forms. *Appl Phys Lett* 2002;80: 586e8.
- [34] Fatemeh Mollaamin, Sara Shahriari, Majid Monajjemi, Zahra Khalaj, Nanocluster of Aluminum Lattice via Organic Inhibitors Coating: A Study of Freundlich Adsorption. *Journal of Cluster Science* 2022, 1-16. <https://doi.org/10.1007/s10876-022-02335-1>.
- [35] Monajjemi, M.; Mollaamin, F.; Gholami, M.R.; Yoosbashizadeh, H.; Sadrnezhad, S.K.; Passdar, H. Quantum Chemical Parameters of Some Organic Corrosion Inhibitors, Pyridine, 2-Picoline 4-Picoline and 2,4-Lutidine, Adsorption at Aluminum Surface in Hydrochloric and Nitric Acids and Comparison Between Two Acidic Media. *Main Group Met. Chem.* **2003**, *26*, 349-362, <https://doi.org/10.1515/MGMC.2003.26.6.349>.
- [36] Dennington R, Keith TA, Millam JM. GaussView. Version 6. Shawnee Mission (KS): Semichem Inc., 2016.
- [37] Frisch, M. J.; Trucks, G. W.; Schlegel, H. B.; Scuseria, G. E.; Robb, M. A.; Cheeseman, J. R.; Scalmani, G.; Barone, V.; Petersson, G. A.; Nakatsuji, H. et al. Gaussian 16, Revision C.01, Gaussian, Inc., Wallingford CT, 2016.
- [38] Perdew, J.P.; Burke, K.; Ernzerhof, M. Generalized Gradient Approximation Made Simple. *Phys. Rev. Lett.* 1996, *77*, 3865.
- [39] Svensson, M.; Humbel, S.; Froese, R.D.J.; Matsubara, T.; Sieber, S.; and Morokuma, K. ONIOM: A Multilayered Integrated MO + MM Method for Geometry Optimizations and Single Point Energy Predictions. A Test for Diels–Alder Reactions and Pt(P(t-Bu)₃)₂ + H₂ Oxidative Addition. *J. Phys. Chem.* **1996**, *100*(50), 19357–19363. <https://doi.org/10.1021/jp962071j>.
- [40] Lehtola, S. A review on non-relativistic fully numerical electronic structure calculations on atoms and diatomic molecules". *Int. J. Quantum Chem.* 2019, *119* (19): e25968. doi:10.1002/qua.25968.
- [41] G Henkelman, A Arnaldsson, and H Jónsson, "A fast and robust algorithm for Bader decomposition of charge density," *Computational Materials Science* 36(3), 354-360 (2006).
- [42] Y G Zhou, X T Zu, F Gao et al., "Electronic and magnetic properties of graphene absorbed with S atom: A first-principles study," *Journal of Applied Physics* 105(10), 104311 (2009).
- [43] Y Mao, J Yuan, and J Zhong, "Density functional calculation of transition metal adatom adsorption on graphene," *Journal of Physics: Condensed Matter* 20(11), 115209 (2008).
- [44] 43. Smith, J. A. S. Nuclear Quadrupole Resonance Spectroscopy. *Journal of Chemical Education.* 48: 39–41, 1971.
- [45] Lucken, E.A.C. Nuclear Quadrupole Coupling Constants; Academic Press Inc.: London, UK; New York, NY, USA, 1969.
- [46] Trontelj, Z.; Pirnat, J.; Jazbinšek, V.; Lužnik, J.; Srčič, S.; Lavrič, Z.; Beguš, S.; Apih, T.; Žagar, V.; Seliger, J. Nuclear Quadrupole Resonance (NQR)—A Useful Spectroscopic Tool in Pharmacy for the Study of Polymorphism. *Crystals* 2020, *10*, 450. <https://doi.org/10.3390/cryst10060450>.

-
- [47] 46. Young, Hugh A.; Freedman, Roger D. (2012). *Sears and Zemansky's University Physics with Modern Physics* (13th ed.). Boston: Addison-Wesley. p. 754.
- [48] 47. El Nokab, M.E.H.; Alassmy, Y.A.; Abduljawad, M.M.; Al-shamrani, K.M.; Alnafisah, M.S.; Asgar Pour, Z.; Tucker, C.L.; Sebakhy, K.O. Solid-State NMR Spectroscopy: Towards Structural Insights into Starch-Based Materials in the Food Industry. *Polymers* 2022, 14, 4686.
<https://doi.org/10.3390/polym14214686>.
- [49] 48. Kazak, A.; Marchenkova, M.; Smirnova, A.; Dubinina, T.; Seregin, A.; Rogachev, A.; Usoltseva, N. Thin-film materials based on phthalocyanine derivatives: Structure and physico-chemical properties. *ITM Web Conf.* 2019, 30, 08006.
<https://doi.org/10.1051/itmconf/20193008006>.
- [50] 49. González-Díaz, J.; García-Martín, A.; Armelles, G.; García-Martín, J.; Clavero, C.; Cebollada, A.; Lukaszew, R.; Skuza, J.; Kumah, D.; Clarke, R. Surface-magnetoplasmon nonreciprocity effects in noble-metal/ferromagnetic heterostructures. *Phys. Rev. B* 2007, 76, 153402.
<https://doi.org/10.1103/PhysRevB.76.153402>.
- [51] 50. Rizal, C. Magneto-Optic Surface Plasmon Resonance Ti/Au/Co/Au/Pc Configuration and Sensitivity. *Magnetochemistry* 2018, 4, 35.
<https://doi.org/10.3390/magnetochemistry4030035>.
- [52] 51. Manera, M.G.; Giancane, G.; Bettini, S.; Valli, L.; Borovkov, V.; Colombelli, A.; Lospinoso, D.; Rella, R. MagnetoPlasmonic Waves/HOMO-LUMO Free π -Electron Transitions Coupling in Organic Macrocycles and Their Effect in Sensing Applications. *Chemosensors* 2021, 9, 272.
<https://doi.org/10.3390/chemosensors9100272>.